1. Supplementary methods

1.1 Husbandry

Hypsibius exemplaris (Gasiorek, Stec, Morek & Michalczyk, 2018) adult strain was sourced from Sciento in 2018. Cultures were kept in 50 ml – 75 ml Chalkley's media (CM; CaCl2 0.006 g/L, KCl 0.004 g/L, NaCl 0.1 g/L in autoclaved ddH2O) at 22 Co in 12h dark – 12h light cycle. Once a month the medium was changed by filtering animals with a (50 µm) mesh and washing off them with fresh media. Animals were fed once every two weeks with 1 ml Chlorococcus sp. algae culture.

1.2 Sampling for RNAseq and cell lysis

Hypsibius exemplaris (Gasiorek, Stec, Morek & Michalczyk, 2018) cultures were monitored for egg-laying events. Egg laying is done in conjunction with molting, therefore right after egg laying the adult exits the cuticle leaving behind the eggs in the shed exuvia. At room temperature, the first cleavage commences after 2 hours post-laying by which time adults have left the exuvia (Gabriel et al., 2007). Before collection surfaces and tools used for the collection were cleaned with RNaseZap and filtered tips were used throughout the collection to avoid RNase contamination. Animals, where the adult and embryos were present together, were selected from the cultures. Staging of embryos was performed under an Axioscope Zeiss microscope with differential interference contrast (DIC) settings. Embryos were dissected from the exuvia with Tungsten needles and washed three times in CM. Afterward, there were transferred into 4.4 µl of lysis solution (2.4 µl of 1:19 Triton-X and RNAse inhibitor 40U/µl from MegaScript T7 transcription kit diluted in nuclease-free water; 1 µl 10mM each dNTP; 1 µl 5 µM oligo-dT) (Picelli, Björklund, et al., 2014; Picelli, Faridani, et al., 2014). Sampled embryos were transferred to PCR strip tubes (one embryo in each tube), labeled, and snap-frozen in liquid nitrogen. In order to crack the eggshell of the embryos three cycles of snap freezing and thawing were used. Snap freezing was achieved with liquid nitrogen, thawing with a 42 Co water bath, and each step lasted 30 seconds. Following this samples were shipped to GeneCore (EMBL Genomics Core Facilities) where RNA extraction and amplification (18 PCR cycles proved to be the most optimal) were performed according to the Smart-Seq2 protocol (Picelli et al., 2014). Sequencing was performed with 75 base pair single-end reads on a single lane of a NextSeq machine.

1.3 RNAseq and associated dataset retrieval

The collection of RNAseq datasets was done manually through SRA-explorer (SRA-explorer) in 2021. NCBI's sequence read archive (SRA) was searched for keywords covering topics related to this project (e.g. "oocyte", "egg", "early development"). Filtering criteria for datasets were the following: reads had to originate from RNAseq experiments, species of origin had to belong to the Metazoa lineage, biological replicates had to be included, and sampling had to cover early development up until gastrulation. If the criteria were met, then the raw fastq files were downloaded. Where possible, genomic resources were also downloaded from Ensembl, NCBI or ParaSite databases.

Sequences generated or retrieved during this project were quality inspected using FastQC. Raw fastq files were trimmed using fastp (Chen et al., 2018). Adapter removal, low-quality nucleotide trimming, low complexity filtering, and base correction with paired-end data were applied. Upon completion, fastq files were inspected again with FastQC. All subsequent applications were done with trimmed fastq files.

1.4 Transcriptome assemblies

In the case of the species where genomic resources were unavailable transcriptomes were *de novo* assembled. An over-assembly approach was chosen as it improves the quality of the assembly (Hölzer & Marz, 2019; Surget-Groba & Montoya-Burgos, 2010). With this approach, multiple assembly software, multiple studies, and multiple k-mer sizes produce a diverse set of contigs. These contigs then can be filtered using various strategies to achieve a final, non-redundant transcriptome. The three main assemblers used were: Trinity, TransAbyss, and RNASpades. K-mer sizes were chosen according to read sizes. After trimming reads had a distribution of varying lengths, the shortest one was used as reference length for k-mer choice. The k-mer had to be of a minimum length of 50% read length and could not exceed 80% read length size. In this range several k-mer values were chosen for different assemblies. A notable exception to this is Trinity, which has a fixed k-mer value of 32.

Assemblies were then concatenated for each species and using the EvidentialGene pipeline further processed (Gilbert, 2019). Non-redundant transcripts are retained and from them, open reading frames are predicted, from which coding sequences and subsequently protein sequences are retrieved. Homology information is also added by aligning coding sequences to the uniprot-swissprot database (Bateman et al., 2021) with the ultrafast diamond aligner (Buchfink et al., 2014). The quality of each assembly was evaluated with BUSCO scores (Simão et al., 2015). This was run in proteome mode and in all cases it was used against the metazoa_odb10 database.

Despite having a published genome, *Hypsibius exemplaris* transcriptome was assembled de novo for use. This was done for two reasons: the current annotation of the genome lacks UTR sequence annotations and the de novo transcriptome assembly improved the mappability of reads considerably during quantification. This discrepancy could be attributed to the lack of embryonic stages during the genome annotation for the genome version nHd3.0 (Yoshida Yuki and Koutsovoulos, 2017). The quality of this transcriptome was of comparable quality to the genome based on BUSCO analysis (Suppl. Figure 5, Suppl. Table 2).

A fixed species tree topology was retrieved from Open Tree of Life (Redelings & Holder, 2017). Branch lengths for this tree were adjusted according to the orthogroups used by OrthoFinder's algorithm to estimate a species phylogeny. These orthogroups were separately realigned, concatenated and used for estimation of branch lengths for the fixed topology species tree (Suppl. Figure 6).

1.5 Quantification and differential gene expression analysis

If genomic sequences were available, then that was used as a decoy during indexing of the cDNA sequences, otherwise, cDNA sequences were indexed directly. Quantifications were done with mapping validation, bias awareness enabled, and bootstrapping.

A separate approach using the zFPKM normalization approach was also tested (Hart et al., 2013). The list of maternal genes proved to be highly similar in the two cases. Due to its simplicity with similar results, the cut-off value was favored for downstream analyses.

Functional enrichment analysis was done in R programming language environment. Functional annotations were either imported from available genomic resources or assigned *de novo*. For the latter two strategies were used: the transcriptome assembly provided homology information was used for inferring gene ontology annotations or a web-service tool Pannzer2 assigned high probability annotations. For the enrichment itself, the clusterProfiler package's enricher() and enrichGO() functions were utilized

(Törönen et al., 2018; Yu et al., 2012). The former was used in cases with custom gene ontological annotation databases built *de novo*, the latter for available annotations. If custom annotations were provided to enricher() as a background set all GO annotations retrieved for all genes per each species were used. All ontological categories were tested and considered enriched with a cut-off value of < 0.05 for the adjusted p-values. Both categories of maternal genes were tested this way separately, ordering of the genes was done by the absolute value of the log2 fold changes in the degraded category and the TPM values for the non-degraded genes. In the case of enrichment of the fitted models, a similar approach was used. The enricher() function was utilized and as a background set all annotated terms for all orthogroups were utilized. Orthogroups were annotated using a custom script and the UniProtKB database was used for homology inference (Bateman et al., 2021). For each orthogroup, GO terms were associated using the UniprotR package (Soudy et al., 2020) .

Information on the lengths of different architectural characteristics of genes were extracted from their genome annotations. Species, where only coding sequence and intron lengths were available, were omitted. Where multiple feature sizes were annotated due to alternative splicing events the means of these lengths were taken. For plotting the mean lengths or proportions were used.

2. Supplemental results

2.1 Transcriptome assemblies

BUSCO scores evaluate the completeness of a predefined gene set characteristic of a lineage against the transcriptome. Based on the BUSCO scores the assembly pipeline resulted in consistently complete transcriptomes (Suppl. Figure 5, Suppl. Table 2). Some species displayed more open reading frames (ORFs) than transcripts, this is a well-known phenomenon during transcriptome assemblies whereby chimeric transcripts are assembled (Gilbert, 2019). Nevertheless, the predicted coding sequences are of reasonable numbers and their annotation based on the UniProt database (Bateman et al., 2021) suggests high quality transcriptomes.

3. Supplementary bibliography

Bateman, A., Martin, M. J., Orchard, S., Magrane, M., Agivetova, R., Ahmad, S., Alpi, E., Bowler-Barnett, E. H., Britto, R., Bursteinas, B., Bye-A-Jee, H., Coetzee, R., Cukura, A., Silva, A. Da, Denny, P., Dogan, T., Ebenezer, T. G., Fan, J., Castro, L. G., … Zhang, J. 2021. UniProt: The universal protein knowledgebase in 2021. *Nucleic Acids Research*, *49*(D1), D480–D489.

Buchfink, B., Xie, C., & Huson, D. H. 2014. Fast and sensitive protein alignment using DIAMOND. *Nature Methods* (Vol. 12, Issue 1, pp. 59–60).

Chen, S., Zhou, Y., Chen, Y., & Gu, J. 2018. fastp: an ultra-fast all-in-one FASTQ preprocessor. *Bioinformatics (Oxford, England)*, *34*(17), i884–i890.

Gabriel, W. N., McNuff, R., Patel, S. K., Gregory, T. R., Jeck, W. R., Jones, C. D., & Goldstein, B. 2007. The tardigrade Hypsibius dujardini, a new model for studying the evolution of development. *Developmental biology*, *312*(2), 545–559.

GĄsiorek, P., Stec, D., Morek, W., & Michalczyk, Ł. 2018. An integrative redescription of Hypsibius dujardini (Doyère, 1840), the nominal taxon for Hypsibioidea (Tardigrada: Eutardigrada). *Zootaxa*, *4415*(1), 45–75.

Gilbert, D. G. 2019. Genes of the pig, Sus scrofa, reconstructed with EvidentialGene. *PeerJ*, *7*, e6374–e6374.

Hart, T., Komori, H. K., LaMere, S., Podshivalova, K., & Salomon, D. R. (2013). Finding the active genes in deep RNA-seq gene expression studies. *BMC genomics*, *14*, 778.

Hölzer, M., & Marz, M. 2019. De novo transcriptome assembly: A comprehensive cross-species comparison of short-read RNA-Seq assemblers. *GigaScience*, *8*(5), giz039.

Picelli, S., Faridani, O. R., Björklund, A. K., Winberg, G., Sagasser, S., & Sandberg, R. 2014. Full-length RNA-seq from single cells using Smart-seq2. *Nature protocols*, *9*(1), 171–181.

OpenTreeOfLife, Redelings, B., Reyes, L. L. S., Cranston, K. A., Allman, J., Holder, M. T., & McTavish, E. J. 2019. *Open Tree of Life Synthetic Tree*. Zenodo.

Simão, F. A., Waterhouse, R. M., Ioannidis, P., Kriventseva, E. v, & Zdobnov, E. M. 2015. BUSCO: assessing genome assembly and annotation completeness with single-copy orthologs. *Bioinformatics*, *31*(19), 3210–3212.

Soudy, M., Anwar, A. M., Ahmed, E. A., Osama, A., Ezzeldin, S., Mahgoub, S., & Magdeldin, S. 2020. UniprotR: Retrieving and visualizing protein sequence and functional information from Universal Protein Resource (UniProt knowledgebase). *Journal of Proteomics*, *213*, 103613.

Surget-Groba, Y., & Montoya-Burgos, J. I. 2010. Optimization of de novo transcriptome assembly from next-generation sequencing data. *Genome Research*, *20*(10), 1432–1440.

Törönen, P., Medlar, A., & Holm, L. 2018. PANNZER2: a rapid functional annotation web server. *Nucleic Acids Research*, *46*(W1), W84–W88.

Yoshida Y, Koutsovoulos G, Laetsch DR, Stevens L, Kumar S, et al. (2017) Comparative genomics of the tardigrades *Hypsibius dujardini* and *Ramazzottius varieornatus*. PLOS Biology 15(7): e2002266.

Yu, G., Wang, L.-G., Han, Y., & He, Q.-Y. 2012. clusterProfiler: an R Package for Comparing Biological Themes Among Gene Clusters. *OMICS: A Journal of Integrative Biology*, *16*(5), 284–287.

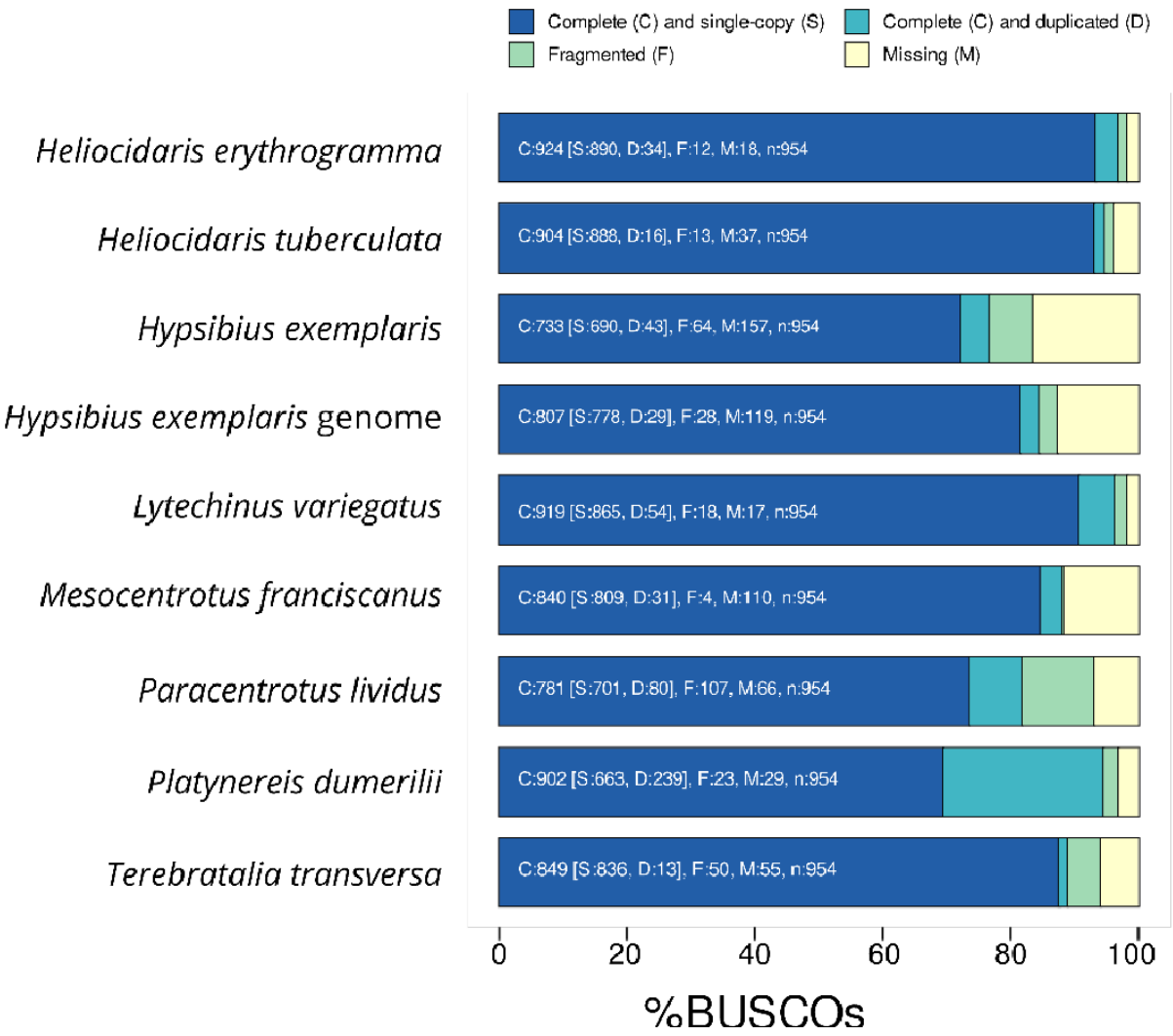

Suppl. figure 5. BUSCO scores distribution of the de novo assembled transcriptomes used in this project.

Species	Transcript number	N50	Longest transcript*	ORF	Coding number	Annotated number
Heliocidaris erythrogramma	102,483	1,530	19,737	105,432	21,403	11,354
Heliocidaris tuberculata	70,765	1,785	20,480	73,370	22,823	12,707
Hypsibius exemplaris	40,568	1,117	11,326	41,790	31,326	16,659
Lytechnius variegatus	105,487	1,565	21,158	108,263	23,742	12,552
Mesocentrotus franciscanus	67,922	2,819	132,566	31,366	30,952	14,508
Paracentrotus lividus	113,651	721	15,574	114,215	25,809	15,534
Platynereis dumerilii	118,615	982	18,083	119,836	36,494	17,758
Terebratalia transversa	32,446	1,501	13,394	32,817	12,565	11,604

Suppl. Table 1. Summary statistics for de novo transcriptome assemblies (ORF – open reading frame). *-in number of nucleotides.

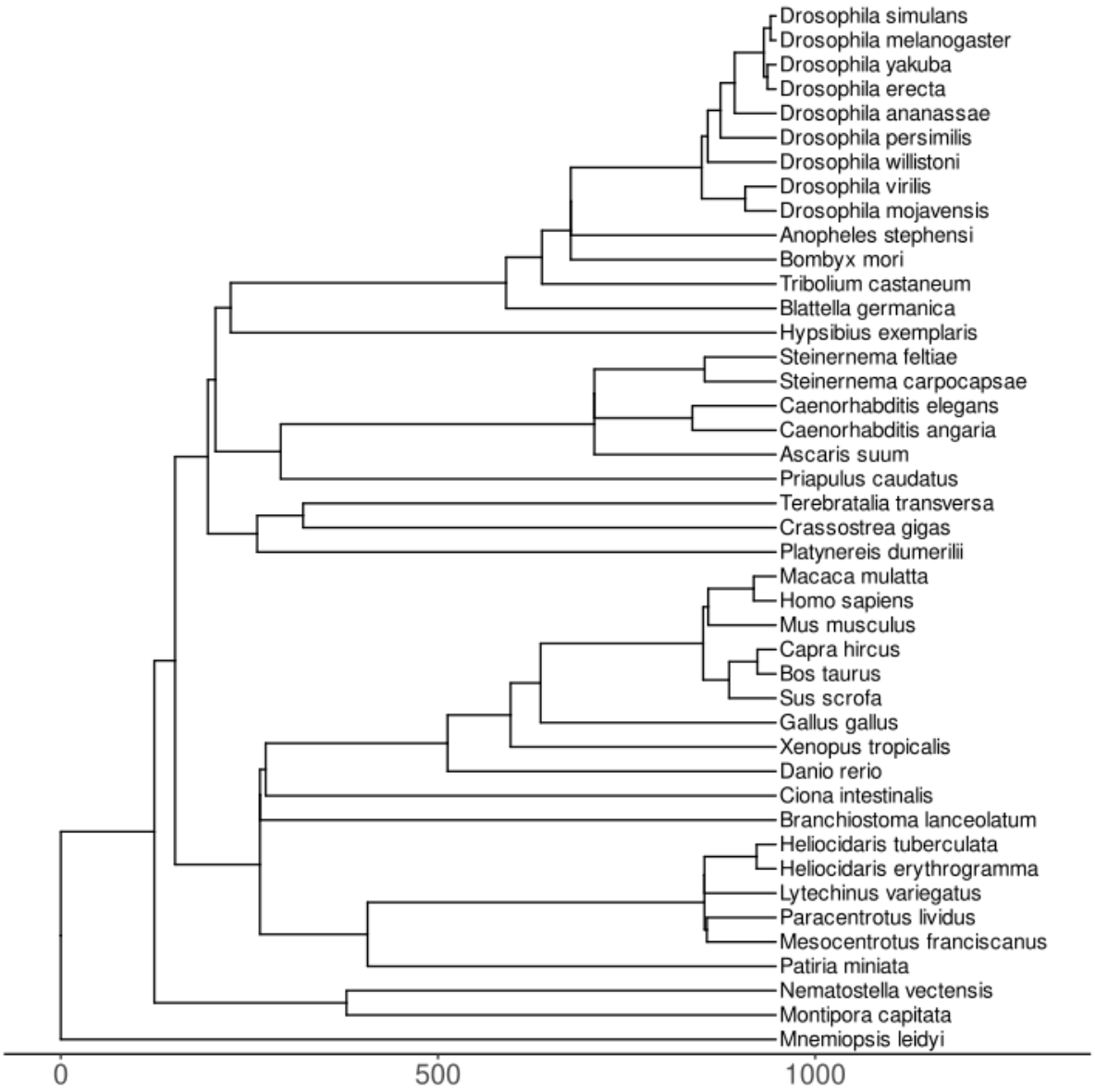

Suppl. Figure 6. Species phylogeny according to ROTL with branch lengths estimated from OrthoFinder and scaled to fossil data from TimeTree. Axis denotes millions of years.

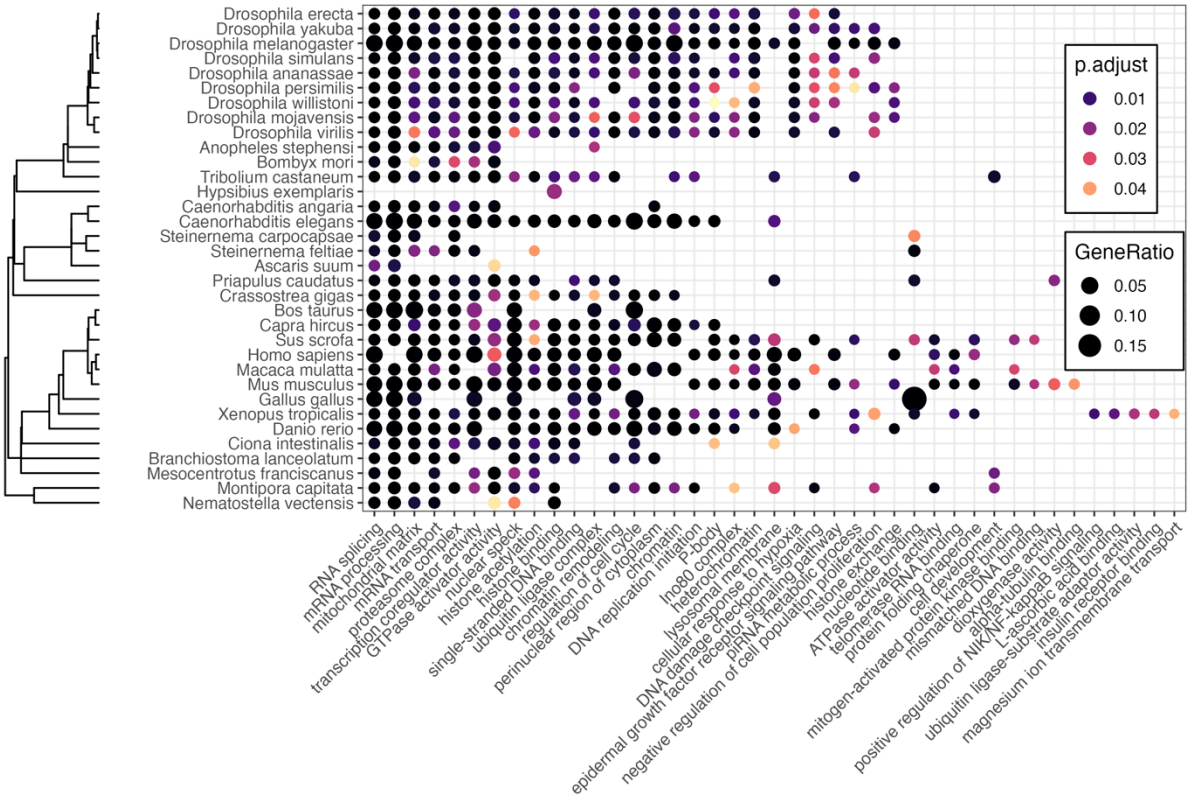

Suppl. figure 7. Gene ontological (GO) enrichment result for maternal genes. (A) On the left each dot represents a significantly enriched GO term in each column, rows represent species.

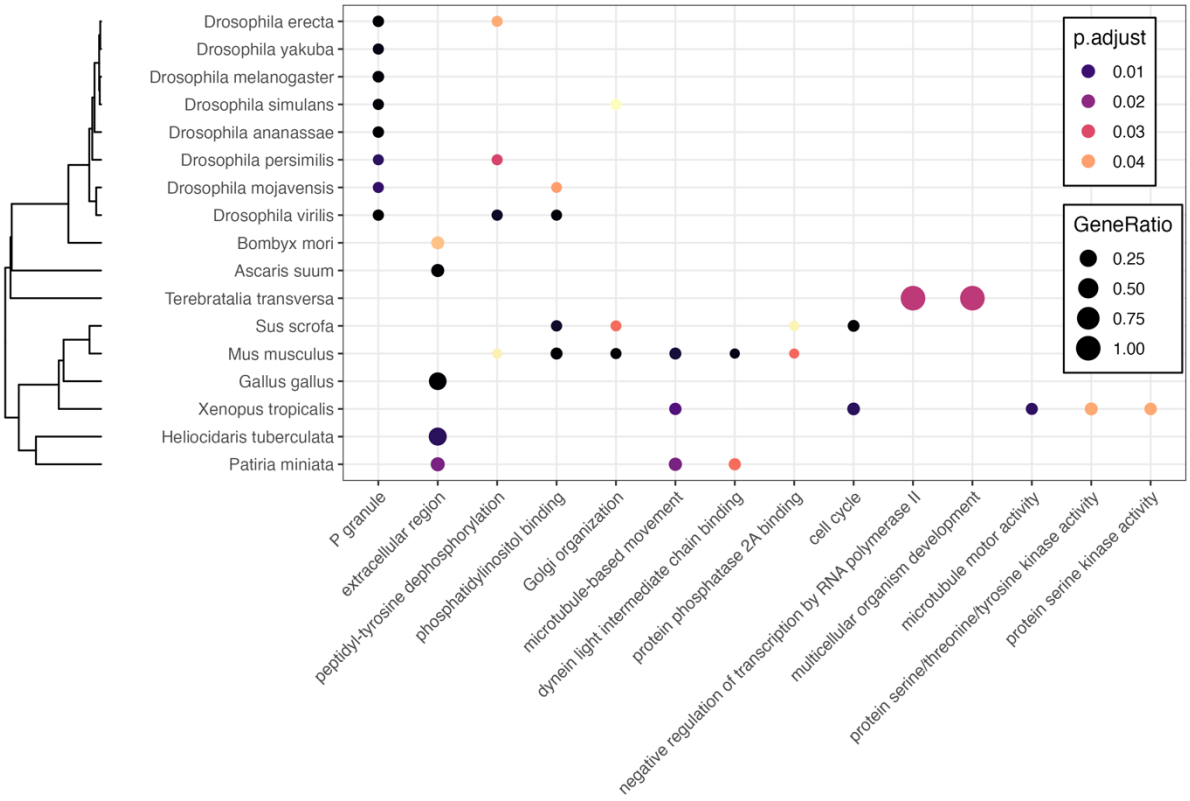

Suppl. figure 8. Gene ontological (GO) enrichment result for degraded maternal genes. (A) On the left each dot represents a significantly enriched GO term in each column, rows represent species.

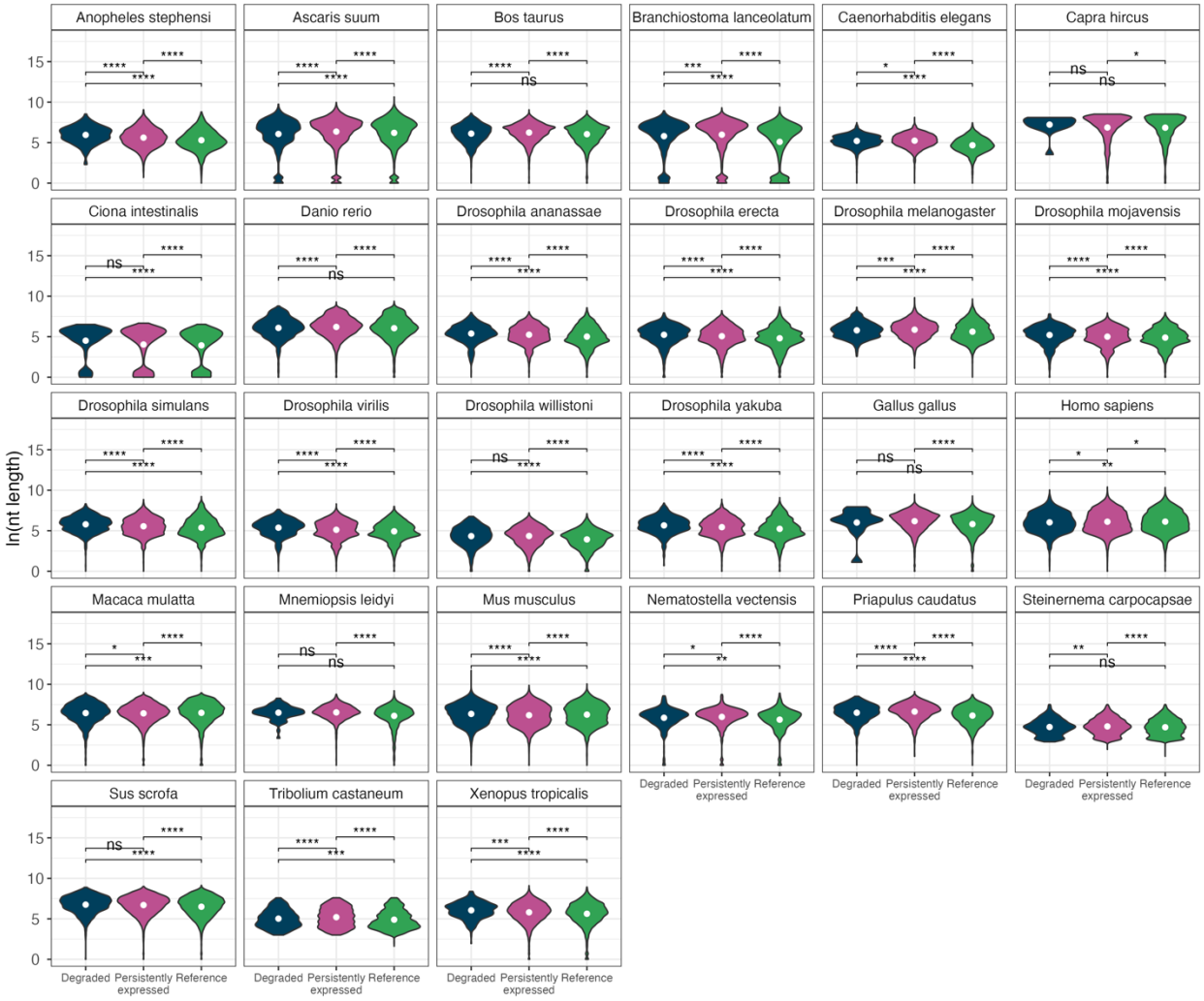

Suppl. Figure 9. Comparison of 3`-UTR lengths across species. Log transformed lengths are compared across species. Maternal genes are subdivided mutually exclusively into degraded maternal genes, maternal genes persistently expressed, and reference genes which don't belong into neither category. White dots represent the medians of the distributions. Adjusted Wilcoxon rank-sum test significances are also displayed. ns – not significant, * = pval < 0.05, ** = pval < 0.01, *** = pval < 0.001 and **** = pval < 10^{-4}

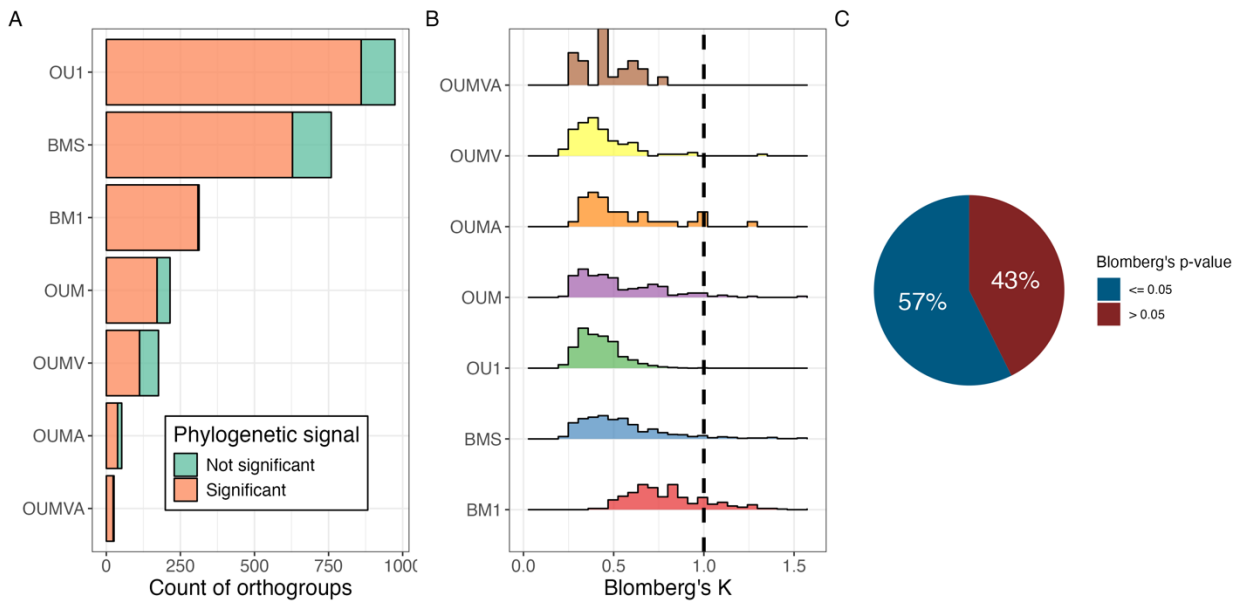

Suppl. figure 10. Phylogenetic signal present in the fitted models. (A) Proportion of orthogroups with significant phylogenetic signal present. (B) The distribution of Blomberg's K value for the orthogroups according to their best fitting evolutionary models. The dashed line represents the expected Blomberg's K value for the Brownian motion model. (C) The proportion of orthogroups with phylogenetic signal present (p-value <= 0.05) or not detected.

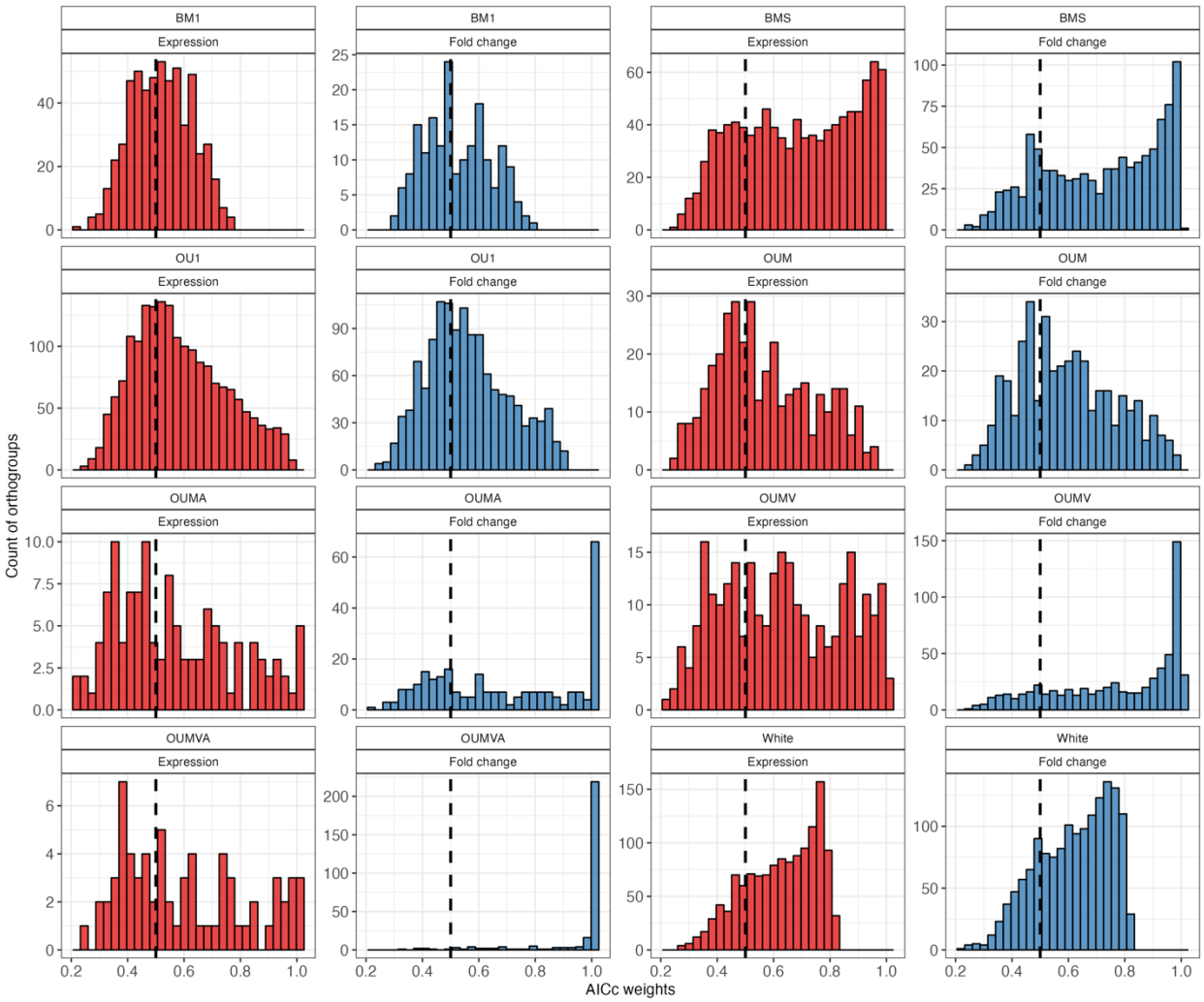

Suppl. Figure 11. AICc distribution after the model fitting process for each tested model. For each orthogroups the best fitting model's AICc was considered. Dashed lines represent the cut-off value used for filtering the best fitting model, together with the permutation test (not shown).

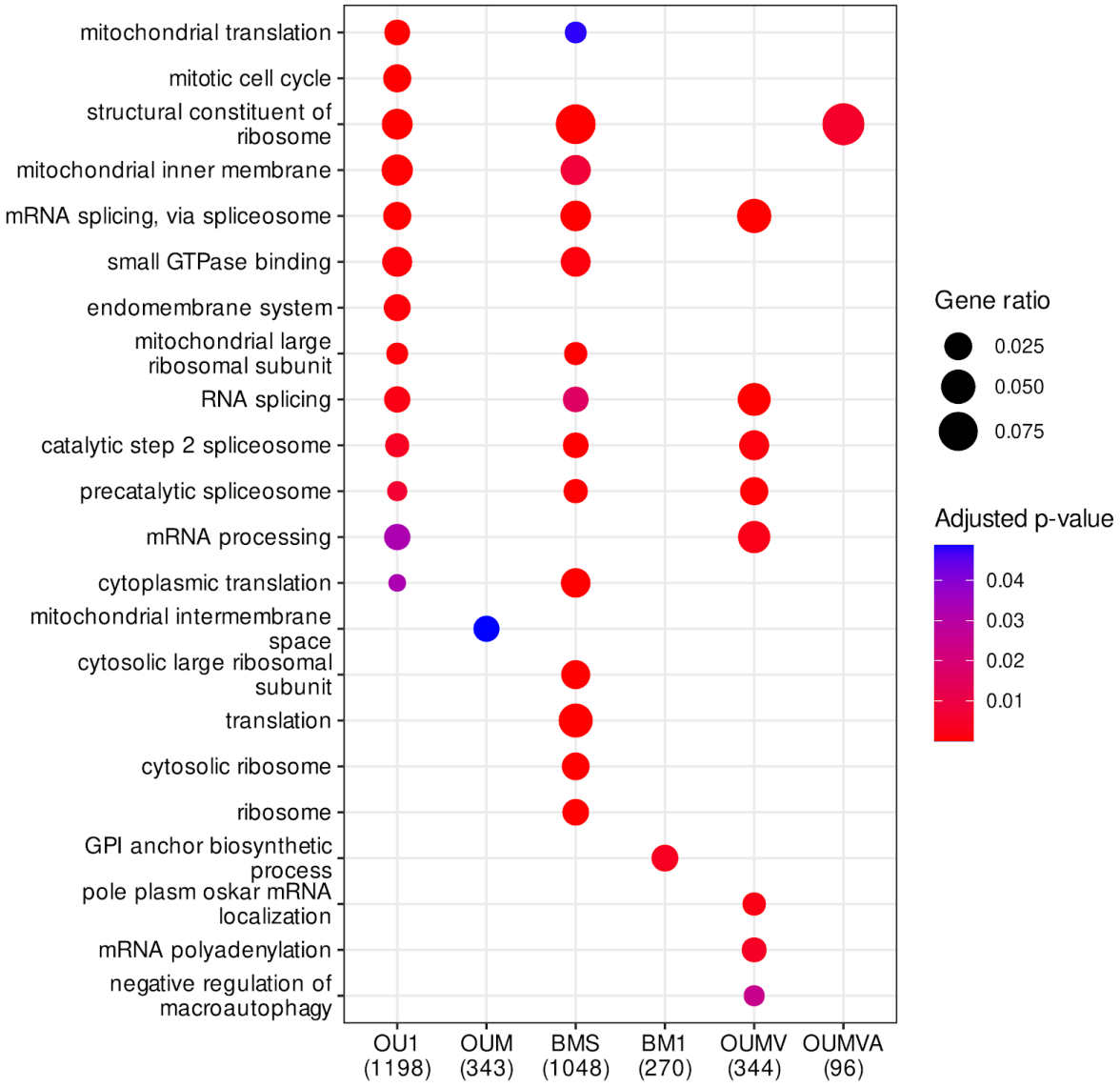

Suppl. Figure 12. Gene ontology terms enriched for each tested evolutionary model.

Model	Category	.y.	group1	group2	n1	n2	statistic	p	p.adj	p.adj.signif
OUM	Expression	value	Hemotrophic Viviparous	Oviparity	194	212	19866	5.55e-01	7.39e-01	ns
OUM	Expression	value	Hemotrophic Viviparous	Ovuliparity	194	214	21155	7.39e-01	7.39e-01	ns
OUM	Expression	value	Oviparity	Ovuliparity	212	214	28719	2.04e-06	6.12e-06	****
OUM	Fold change	value	Hemotrophic Viviparous	Oviparity	228	257	37991	1.67e-08	2.51e-08	****
OUM	Fold change	value	Hemotrophic Viviparous	Ovuliparity	228	258	39411	9.72e-11	2.92e-10	****
OUM	Fold change	value	Oviparity	Ovuliparity	257	258	38156	3.00e-03	3.00e-03	**
OUMA	Expression	value	Hemotrophic Viviparous	Oviparity	41	46	841	3.90e-01	3.90e-01	ns
OUMA	Expression	value	Hemotrophic Viviparous	Ovuliparity	41	52	1223	2.26e-01	3.39e-01	ns
OUMA	Expression	value	Oviparity	Ovuliparity	46	52	1839	4.79e-06	1.44e-05	****
OUMA	Fold change	value	Hemotrophic Viviparous	Oviparity	109	126	7160	5.74e-01	5.74e-01	ns
OUMA	Fold change	value	Hemotrophic Viviparous	Ovuliparity	109	128	7892	8.20e-02	1.23e-01	ns
OUMA	Fold change	value	Oviparity	Ovuliparity	126	128	9314	3.30e-02	9.80e-02	ns
OUMV	Expression	value	Hemotrophic Viviparous	Oviparity	168	174	12393	1.50e-02	2.20e-02	*
OUMV	Expression	value	Hemotrophic Viviparous	Ovuliparity	168	176	13800	2.86e-01	2.86e-01	ns
OUMV	Expression	value	Oviparity	Ovuliparity	174	176	18332	1.00e-03	4.00e-03	**
OUMV	Fold change	value	Hemotrophic Viviparous	Oviparity	269	283	39774	3.61e-01	5.41e-01	ns
OUMV	Fold change	value	Hemotrophic Viviparous	Ovuliparity	269	283	37365	7.09e-01	7.09e-01	ns
OUMV	Fold change	value	Oviparity	Ovuliparity	283	283	36572	7.40e-02	2.23e-01	ns
OUMVA	Expression	value	Hemotrophic Viviparous	Oviparity	25	25	206	3.90e-02	5.80e-02	ns
OUMVA	Expression	value	Hemotrophic Viviparous	Ovuliparity	25	26	311	8.01e-01	8.01e-01	ns
OUMVA	Expression	value	Oviparity	Ovuliparity	25	26	448	2.00e-02	5.80e-02	ns
OUMVA	Fold change	value	Hemotrophic Viviparous	Oviparity	81	91	3691	9.88e-01	9.88e-01	ns
OUMVA	Fold change	value	Hemotrophic Viviparous	Ovuliparity	81	95	4260	2.21e-01	5.64e-01	ns
OUMVA	Fold change	value	Oviparity	Ovuliparity	91	95	4648	3.76e-01	5.64e-01	ns

Suppl. Table 2. Table displaying results of Wilcoxon rank-sum test over all the Θ estimates for all extended Ornstein-Uhlenbeck models. All pairwise comparisons between reproductive modes are included.

group1	group2	effsize	Model	Category	n1	n2	magnitude
Hemotrophic Viviparous	Oviparity	0.029330335	OUM	Expression	194	212	small
Hemotrophic Viviparous	Ovuliparity	0.016522724	OUM	Expression	194	214	small
Oviparity	Ovuliparity	0.230130586	OUM	Expression	212	214	small
Hemotrophic Viviparous	Oviparity	0.256234329	OUM	Fold change	228	257	small
Hemotrophic Viviparous	Ovuliparity	0.293553525	OUM	Fold change	228	258	small
Oviparity	Ovuliparity	0.130561835	OUM	Fold change	257	258	small
Hemotrophic Viviparous	Oviparity	0.092986305	OUMA	Expression	41	46	small
Hemotrophic Viviparous	Ovuliparity	0.125977004	OUMA	Expression	41	52	small
Oviparity	Ovuliparity	0.462370772	OUMA	Expression	46	52	moderate
Hemotrophic Viviparous	Oviparity	0.036777163	OUMA	Fold change	109	126	small
Hemotrophic Viviparous	Ovuliparity	0.113111351	OUMA	Fold change	109	128	small
Oviparity	Ovuliparity	0.133975142	OUMA	Fold change	126	128	small
Hemotrophic Viviparous	Oviparity	0.131504528	OUMV	Expression	168	174	small
Hemotrophic Viviparous	Ovuliparity	0.057542136	OUMV	Expression	168	176	small
Oviparity	Ovuliparity	0.170560723	OUMV	Expression	174	176	small
Hemotrophic Viviparous	Oviparity	0.038869794	OUMV	Fold change	269	283	small
Hemotrophic Viviparous	Ovuliparity	0.015872874	OUMV	Fold change	269	283	small
Oviparity	Ovuliparity	0.075032030	OUMV	Fold change	283	283	small
Hemotrophic Viviparous	Oviparity	0.292233589	OUMVA	Expression	25	25	small
Hemotrophic Viviparous	Ovuliparity	0.036938157	OUMVA	Expression	25	26	small
Oviparity	Ovuliparity	0.324528092	OUMVA	Expression	25	26	moderate
Hemotrophic Viviparous	Oviparity	0.001286696	OUMVA	Fold change	81	91	small
Hemotrophic Viviparous	Ovuliparity	0.092296955	OUMVA	Fold change	81	95	small
Oviparity	Ovuliparity	0.065025525	OUMVA	Fold change	91	95	small

Suppl. Table 3. Table displaying effect size results of Wilcoxon rank-sum test over all the Θ estimates for all extended Ornstein-Uhlenbeck models. All pairwise comparisons between reproductive modes are included. Magnitudes of the effect sizes are determined according to Cohen (1988).

mode	Category	Highest estimated optima	Lowest estimated optima	test_stat	p_val
Hemotrophic Viviparous	Expression	80	78	0.02531646	8.735811e-01
Hemotrophic Viviparous	Fold change	121	55	24.75000000	6.526880e-07
Oviparity	Expression	66	37	8.16504854	4.270533e-03
Oviparity	Fold change	90	92	0.02197802	8.821456e-01
Ovuliparity	Expression	68	99	5.75449102	1.644656e-02
Ovuliparity	Fold change	47	111	25.92405063	3.551171e-07

Table 4. Table containing the results of Pearson's χ^2 test for determining if there is a bias towards having highest or lowest optima within each reproductive mode in OUM models.

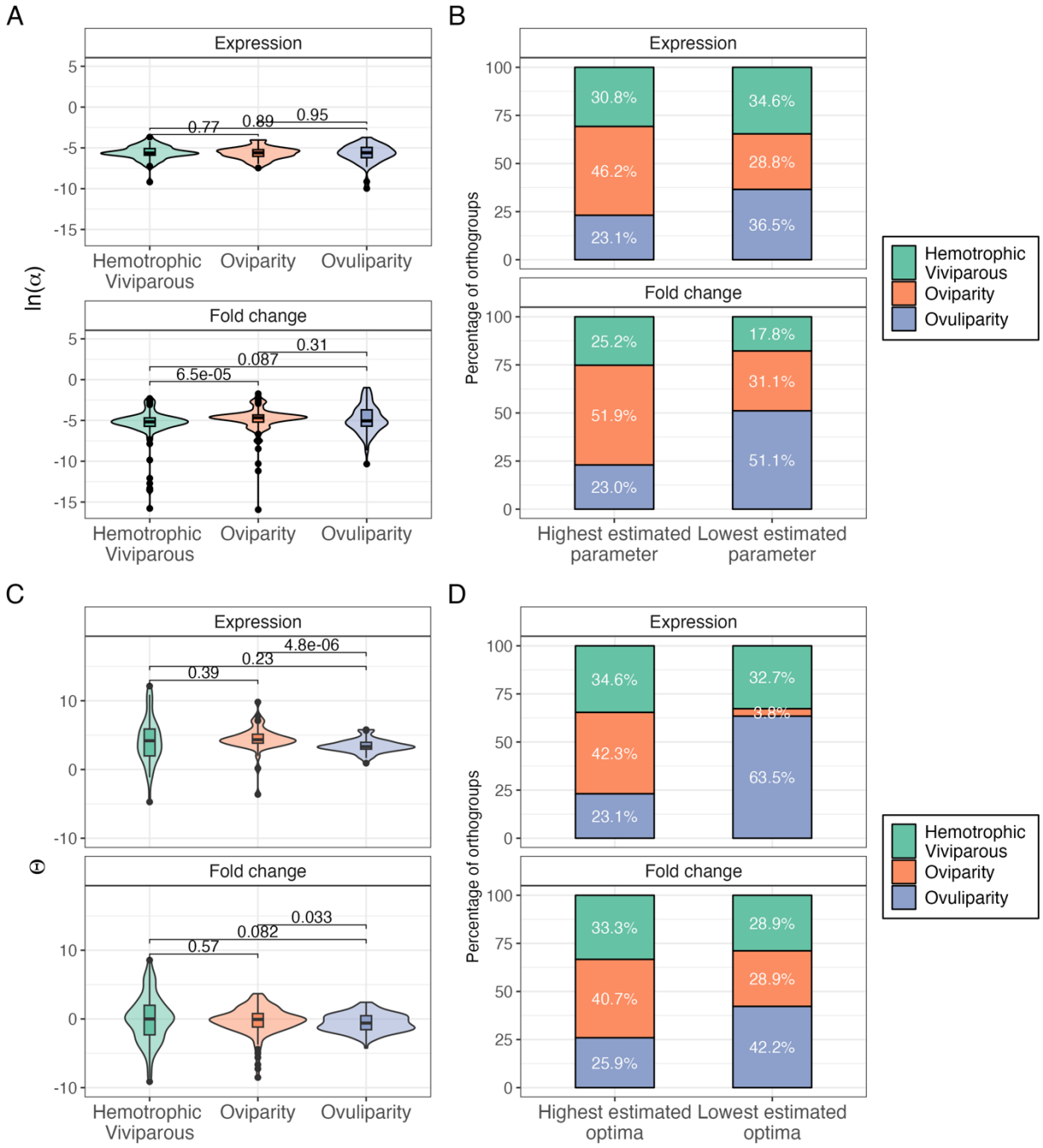

Suppl. figure 13. Parameter estimates for orthogroups where OUMA models were found to be the best fitting model. (A) Distribution of α estimates for the reproductive modes in both expression dataset (above) and fold change dataset (below). (B) The relative number of highest and lowest α values for both datasets in all three reproductive modes. (C) Distribution of Θ estimates for the reproductive modes in both expression dataset (above) and fold change dataset (below). (E) The number of highest and lowest Θ values for both datasets in all three reproductive modes. Wilcoxon rank-sum test results are displayed above (A) and (C) for comparisons of parameter estimates across reproductive modes.

A

Model	Category	group1	group2	n1	n2	statistic	p	p.adj	p.adj.signif
OUMA	Expression	Hemotrophic Viviparous	Oviparity	50	47	1216	7.70e-01	0.946000	ns
OUMA	Expression	Hemotrophic Viviparous	Ovuliparity	50	47	1195	8.88e-01	0.946000	ns
OUMA	Expression	Oviparity	Ovuliparity	47	47	1095	9.46e-01	0.946000	ns
OUMA	Fold change	Hemotrophic Viviparous	Oviparity	114	128	5124	6.48e-05	0.000194	***
OUMA	Fold change	Hemotrophic Viviparous	Ovuliparity	114	130	6469	8.70e-02	0.131000	ns
OUMA	Fold change	Oviparity	Ovuliparity	128	130	8932	3.08e-01	0.308000	ns

B

group1	group2	effsize	Model	Category	n1	n2	magnitude
Hemotrophic Viviparous	Oviparity	0.03004980	OUMA	Expression	50	47	small
Hemotrophic Viviparous	Ovuliparity	0.01465844	OUMA	Expression	50	47	small
Oviparity	Ovuliparity	0.00740953	OUMA	Expression	47	47	small
Hemotrophic Viviparous	Oviparity	0.25685156	OUMA	Fold change	114	128	small
Hemotrophic Viviparous	Ovuliparity	0.10951616	OUMA	Fold change	114	130	small
Oviparity	Ovuliparity	0.06357782	OUMA	Fold change	128	130	small

Suppl. Table 5. Tables for Wilcoxon rank-sum test results between parameter comparisons for OUMA models. P-values are found in (A) and the effect sizes in (B).

mode	Category	Highest estimated optima	Lowest estimated optima	test_stat	p_val
Hemotrophic□ Viviparous	Expression	16	18	0.1176471	0.7316005890
Hemotrophic□ Viviparous	Fold change	34	24	1.7241379	0.1891612726
Oviparity	Expression	24	15	2.0769231	0.1495413546
Oviparity	Fold change	70	42	7.0000000	0.0081509716
Ovuliparity	Expression	12	19	1.5806452	0.2086677877
Ovuliparity	Fold change	31	69	14.4400000	0.0001446961

Suppl. Table 6. Table containing the results of Pearson's χ^2 test for determining if there is a bias towards having highest or lowest α estimates within each reproductive mode in OUMA models.

mode	Category	Highest estimated optima	Lowest estimated optima	test_stat	p_val
Hemotrophic□ Viviparous	Expression	18	17	0.02857143	8.657724e-01
Hemotrophic□ Viviparous	Fold change	45	39	0.42857143	5.126908e-01
Oviparity	Expression	22	2	16.66666667	4.455709e-05
Oviparity	Fold change	55	39	2.72340426	9.888691e-02
Ovuliparity	Expression	12	33	9.80000000	1.745119e-03
Ovuliparity	Fold change	35	57	5.26086957	2.181012e-02

Suppl. Table 7. Table containing the results of Pearson's χ^2 test for determining if there is a bias towards having highest or lowest optima within each reproductive mode in OUMA models.

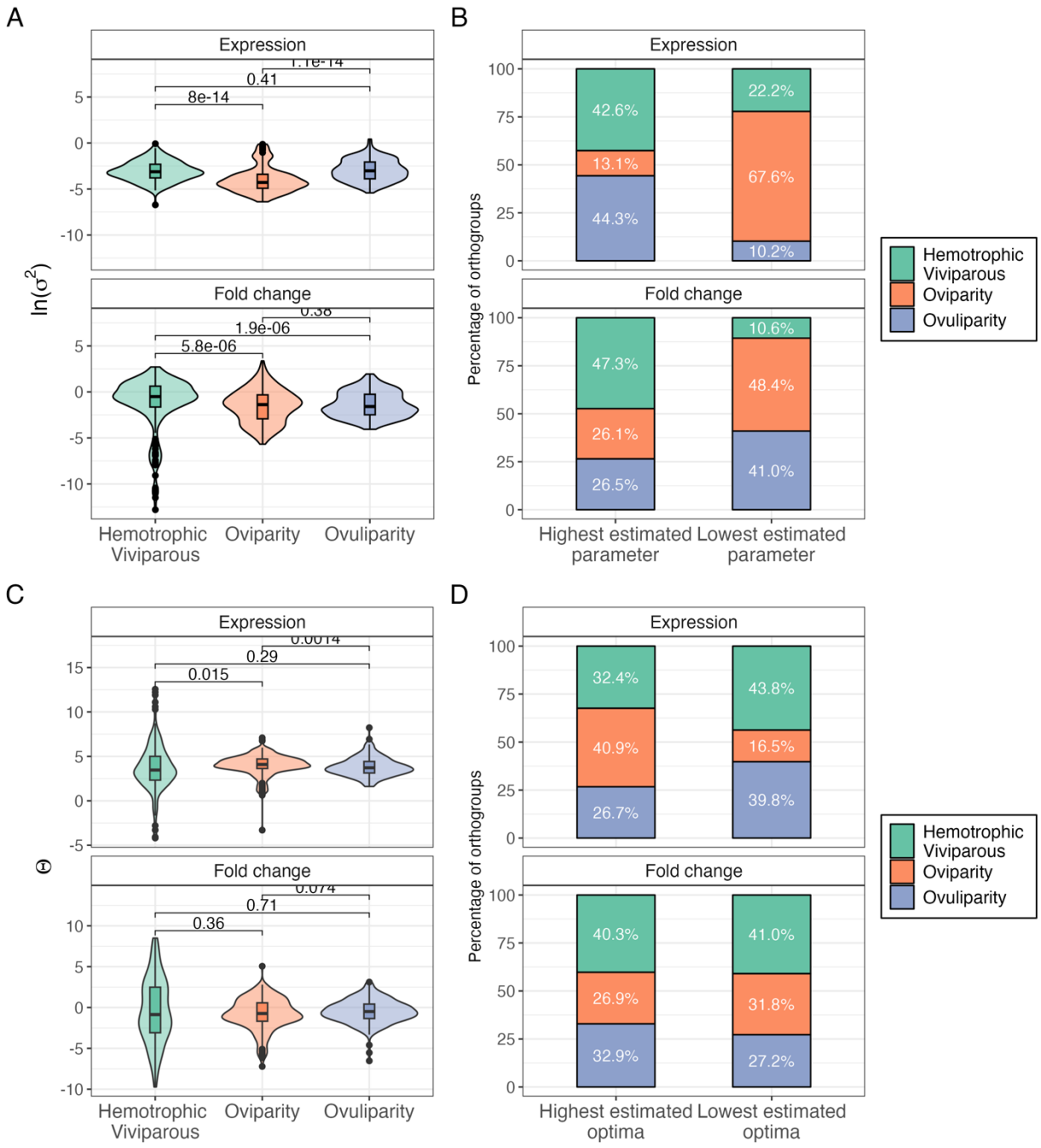

Suppl. Figure 14. Parameter estimates for orthogroups where OUMV models were found to be the best fitting model. (A) Distribution of σ^2 estimates for the reproductive modes in both expression dataset (above) and fold change dataset (below). (B) The relative number of highest and lowest σ^2 values for both datasets in all three reproductive modes. (C) Distribution of Θ estimates for the reproductive modes in both expression dataset (above) and fold change dataset (below). (E) The number of highest and lowest Θ values for both datasets in all three reproductive modes. Wilcoxon rank-sum test results are displayed above (A) and (C) for comparisons of parameter estimates across reproductive modes.

A

Model	Category	group1	group2	n1	n2	statistic	p	p.adj	p.adj.signif
OUMV	Expression	Hemotrophic Viviparous	Oviparity	173	175	22147	8.05e-14	1.21e-13	****
OUMV	Expression	Hemotrophic Viviparous	Ovuliparity	173	176	14439	4.05e-01	4.05e-01	ns
OUMV	Expression	Oviparity	Ovuliparity	175	176	8056	1.11e-14	3.33e-14	****
OUMV	Fold change	Hemotrophic Viviparous	Oviparity	196	279	34017	5.85e-06	8.78e-06	****
OUMV	Fold change	Hemotrophic Viviparous	Ovuliparity	196	283	34833	1.88e-06	5.64e-06	****
OUMV	Fold change	Oviparity	Ovuliparity	279	283	37771	3.75e-01	3.75e-01	ns

B

group1	group2	effsize	Model	Category	n1	n2	magnitude
Hemotrophic Viviparous	Oviparity	0.40043613	OUMV	Expression	173	175	moderate
Hemotrophic Viviparous	Ovuliparity	0.04458966	OUMV	Expression	173	176	small
Oviparity	Ovuliparity	0.41240417	OUMV	Expression	175	176	moderate
Hemotrophic Viviparous	Oviparity	0.20795122	OUMV	Fold change	196	279	small
Hemotrophic Viviparous	Ovuliparity	0.21776003	OUMV	Fold change	196	283	small
Oviparity	Ovuliparity	0.03742257	OUMV	Fold change	279	283	small

Suppl. Table 8. Tables for Wilcoxon rank-sum test results between parameter comparisons for OUMV models. P-values are found in (A) and the effect sizes in (B).

mode	Category	Highest estimated parameter	Lowest estimated parameter	test_stat	p_val
Hemotrophic Viviparous	Expression	75	39	11.368421	7.470336e-04
Hemotrophic Viviparous	Fold change	134	30	65.951220	4.622223e-16
Oviparity	Expression	23	119	64.901408	7.874077e-16
Oviparity	Fold change	74	137	18.810427	1.443757e-05
Ovuliparity	Expression	78	18	37.500000	9.141298e-10
Ovuliparity	Fold change	75	116	8.801047	3.010577e-03

Suppl. Table 9. Table containing the results of Pearson's χ^2 test for determining if there is a bias towards having highest or lowest σ^2 estimates within each reproductive mode in OUMV models.

mode	Category	Highest estimated optima	Lowest estimated optima	test_stat	p_val
Hemotrophic Viviparous	Expression	57	77	2.9850746	8.403541e-02
Hemotrophic Viviparous	Fold change	114	116	0.0173913	8.950823e-01
Oviparity	Expression	72	29	18.3069307	1.880219e-05
Oviparity	Fold change	76	90	1.1807229	2.772089e-01
Ovuliparity	Expression	47	70	4.5213675	3.347407e-02
Ovuliparity	Fold change	93	77	1.5058824	2.197685e-01

Suppl. Table 10. Table containing the results of Pearson's χ^2 test for determining if there is a bias towards having highest or lowest optima within each reproductive mode in OUMV models.

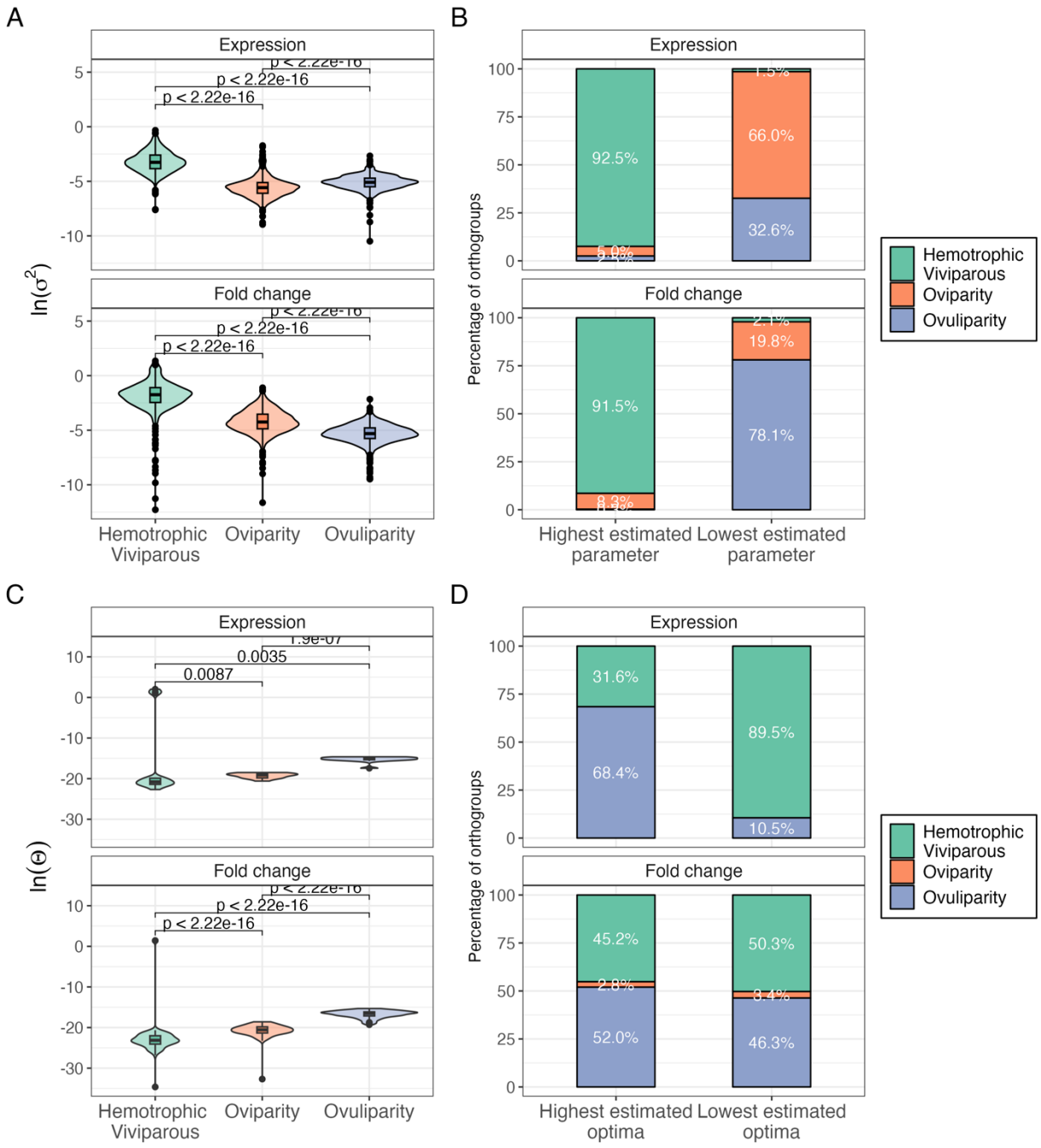

Suppl. Figure 15. Parameter estimates for orthogroups where BMS models were found to be the best fitting model. (A) Distribution of σ^2 estimates for the reproductive modes in both expression dataset (above) and fold change dataset (below). (B) The relative number of highest and lowest σ^2 values for both datasets in all three reproductive modes. (C) Distribution of Θ estimates for the reproductive modes in both expression dataset (above) and fold change dataset (below). (E) The number of highest and lowest Θ values for both datasets in all three reproductive modes. Wilcoxon rank-sum test results are displayed above (A) and (C) for comparisons of parameter estimates across reproductive modes.

A

Model	Category	group1	group2	n1	n2	statistic	p	p.adj	p.adj.signif
BMS	Expression	Hemotrophic Viviparous	Oviparity	748	754	537805	1.83e-203	2.74e-203	****
BMS	Expression	Hemotrophic Viviparous	Ovuliparity	748	758	543916	3.83e-209	1.15e-208	****
BMS	Expression	Oviparity	Ovuliparity	754	758	177641	3.67e-37	3.67e-37	****
BMS	Fold change	Hemotrophic Viviparous	Oviparity	743	752	522324	2.65e-186	3.98e-186	****
BMS	Fold change	Hemotrophic Viviparous	Ovuliparity	743	759	550769	1.85e-224	5.55e-224	****
BMS	Fold change	Oviparity	Ovuliparity	752	759	460765	5.16e-95	5.16e-95	****

B

group1	group2	effsize	Model	Category	n1	n2	magnitude
Hemotrophic Viviparous	Oviparity	0.40043613	OUMV	Expression	173	175	moderate
Hemotrophic Viviparous	Ovuliparity	0.04458966	OUMV	Expression	173	176	small
Oviparity	Ovuliparity	0.41240417	OUMV	Expression	175	176	moderate
Hemotrophic Viviparous	Oviparity	0.20795122	OUMV	Fold change	196	279	small
Hemotrophic Viviparous	Ovuliparity	0.21776003	OUMV	Fold change	196	283	small
Oviparity	Ovuliparity	0.03742257	OUMV	Fold change	279	283	small

Suppl. Table 11. Tables for Wilcoxon rank-sum test results between σ^2 parameter comparisons for BMS models. P-values are found in (A) and the effect sizes in (B).

mode	Category	Highest estimated parameter	Lowest estimated parameter	test_stat	p_val
Hemotrophic Viviparous	Expression	701	11	668.67978	1.935154e-147
Hemotrophic Viviparous	Fold change	696	16	649.43820	2.959996e-143
Oviparity	Expression	38	500	396.73606	2.827878e-88
Oviparity	Fold change	63	151	36.18692	1.792701e-09
Ovuliparity	Expression	19	247	195.42857	2.077191e-44
Ovuliparity	Fold change	2	594	588.02685	6.731299e-130

Suppl. Table 12. Table containing the results of Pearson's χ^2 test for determining if there is a bias towards having highest or lowest σ^2 estimates within each reproductive mode in BMS models.

mode	Category	Highest estimated optima	Lowest estimated optima	test_stat	p_val
Hemotrophic Viviparous	Expression	6	17	5.26086957	0.021810119
Hemotrophic Viviparous	Fold change	80	89	0.47928994	0.488744120
Oviparity	Fold change	5	6	0.09090909	0.763024601
Ovuliparity	Expression	13	2	8.06666667	0.004508698
Ovuliparity	Fold change	92	82	0.57471264	0.448392291

Suppl. Table 13. Table containing the results of Pearson's χ^2 test for determining if there is a bias towards having highest or lowest optima within each reproductive mode in BMS models.

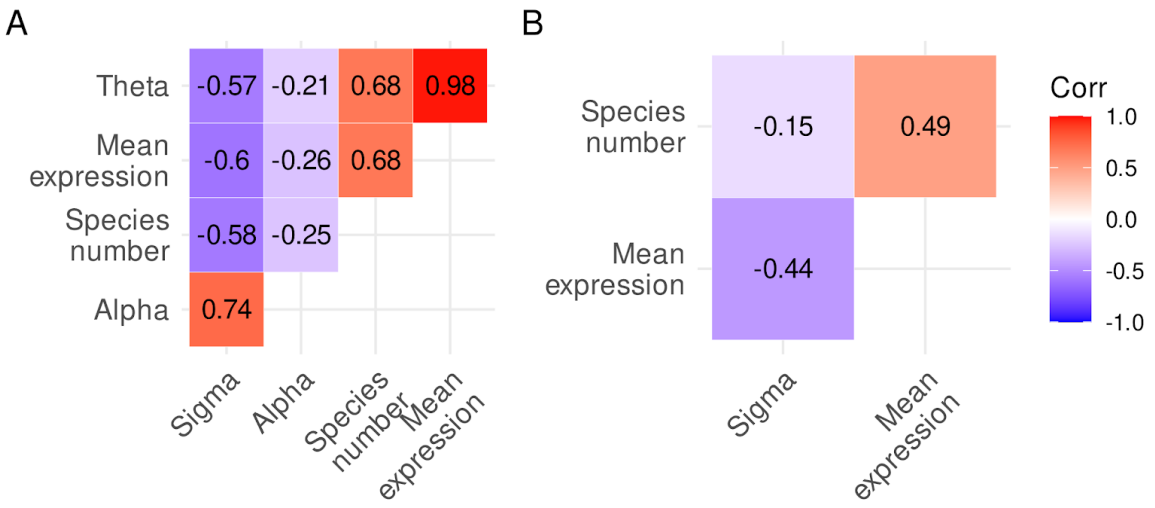

Suppl. Figure 16. Correlation heatmap of parameter estimates for single-regime models. (A) Correlation structure of parameters for the OU1 models. (B) Correlation structure for the BM1 models.

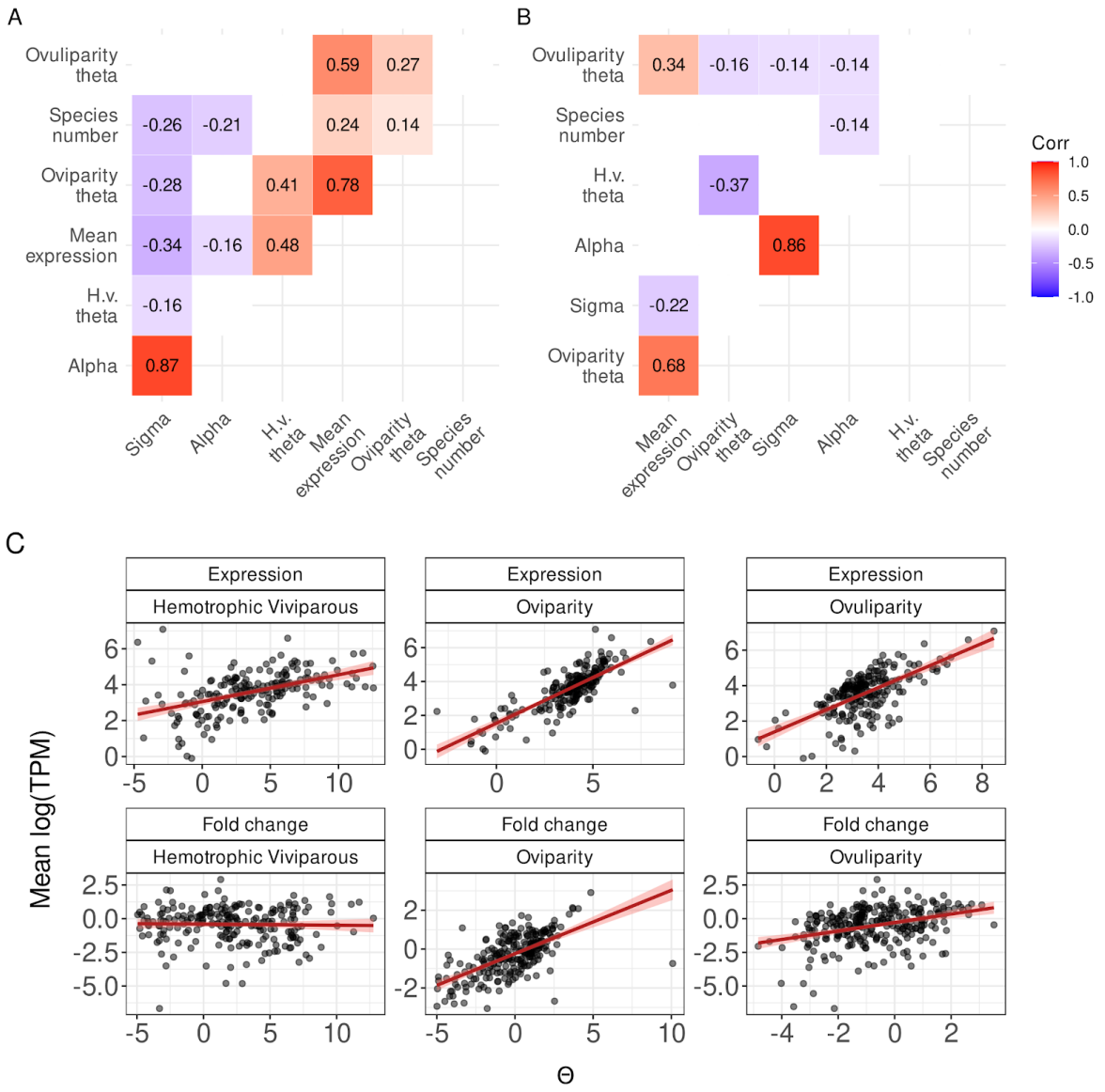

Suppl. Figure 17. Correlation structure of parameter estimates and other variables for OUM models. (A) Correlation structure for expression data following OUM models. Correlation coefficients without p-values < 0.05 are not displayed in cells. (B) Correlation structure for fold change data following OUM models. (C) Linear relationship between mean expression within orthogroups and the OUM Θ estimates for all reproductive modes and data types (expression and fold change).

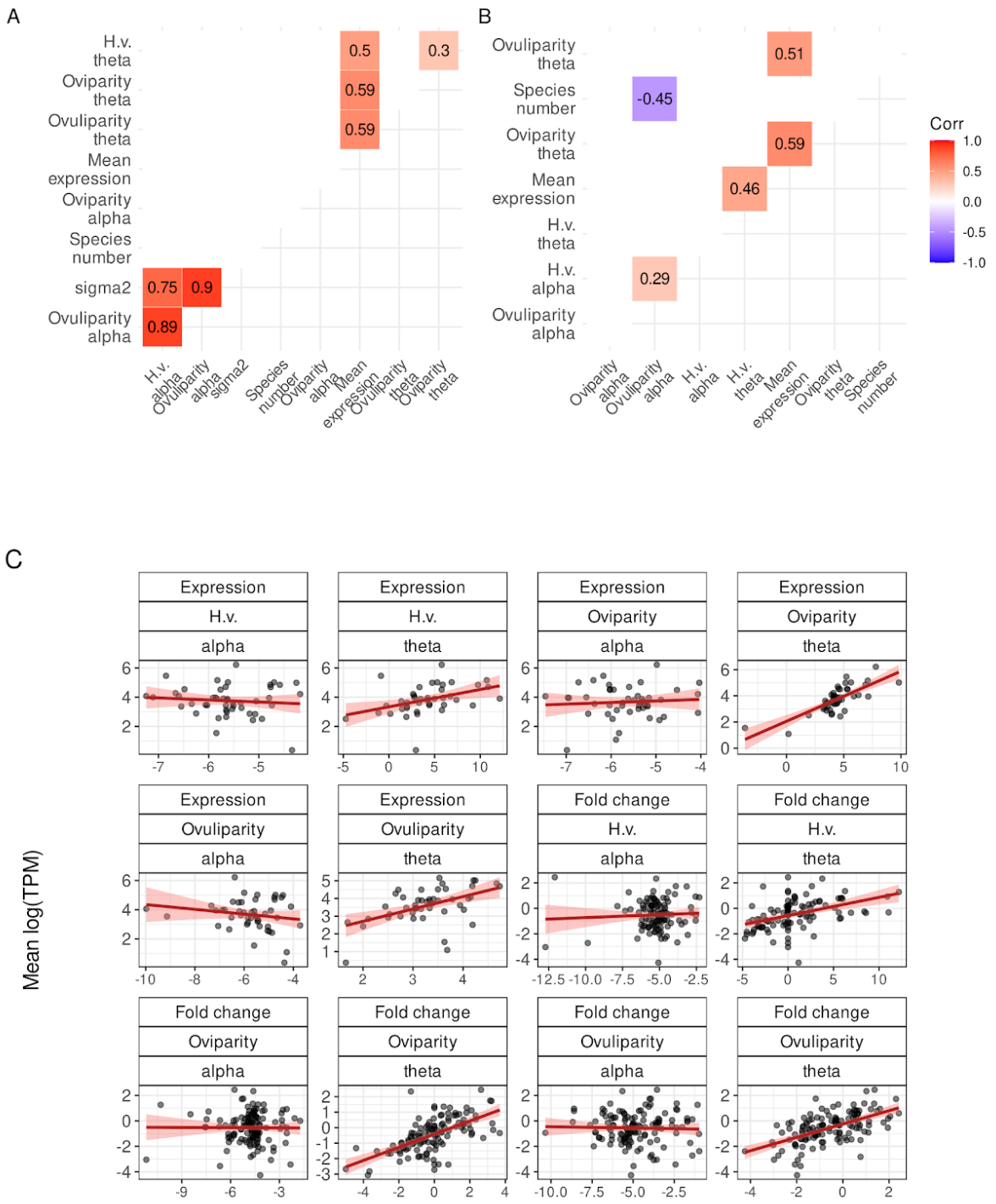

Suppl. Figure 18. Correlation structure of parameter estimates and other variables for OUMA models. (A) Correlation structure for expression data following OUMA models. Correlation coefficients without p-values < 0.05 are not displayed in cells. (B) Correlation structure for fold change data following OUMA models. (C) Linear relationship between mean expression within orthogroups and the OUMA parameter estimates for all reproductive modes and data types (expression and fold change).

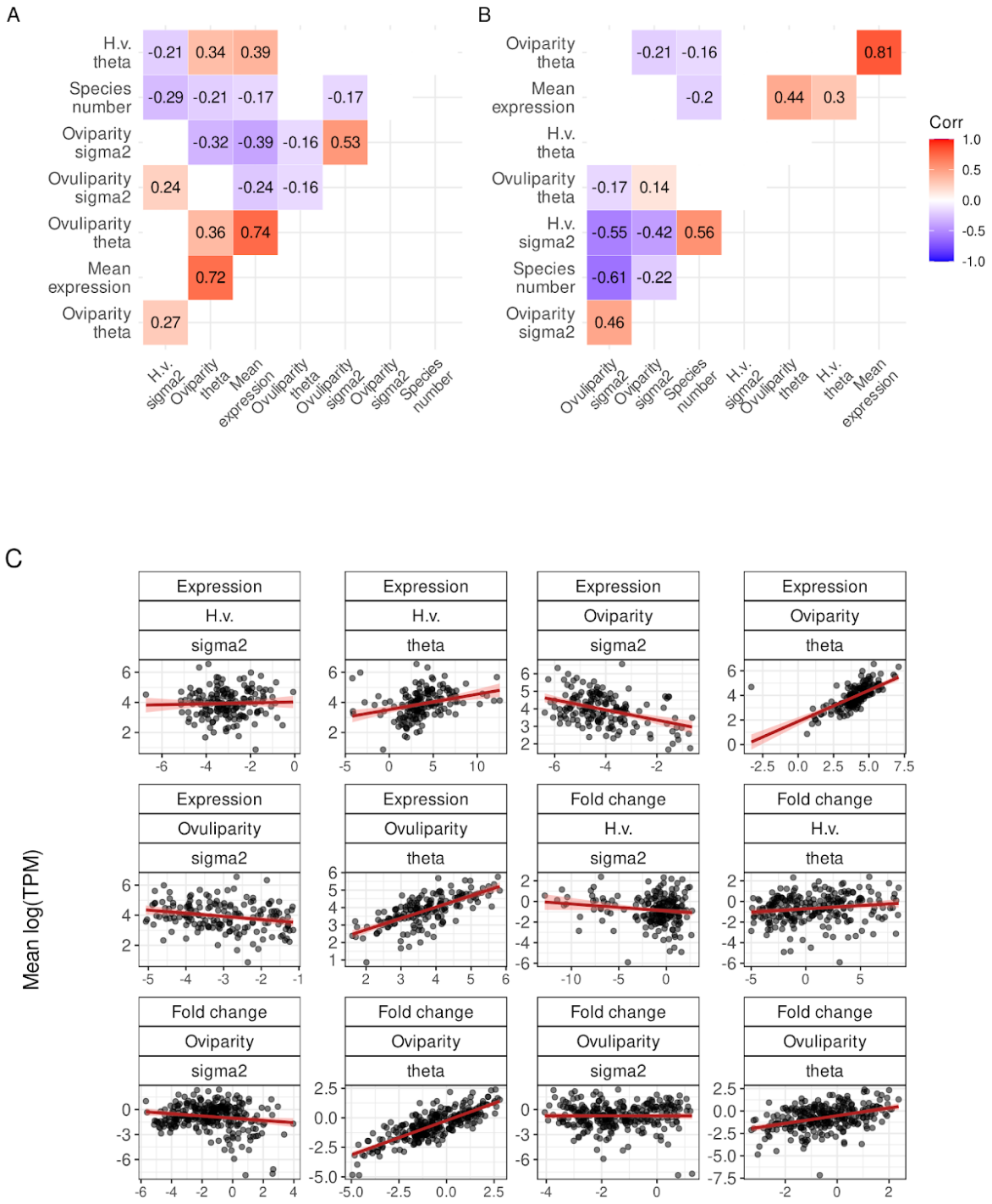

Suppl. Figure 19. Correlation structure of parameter estimates and other variables for OUMV models. (A) Correlation structure for expression data following OUMV models. Correlation coefficients without p-values < 0.05 are not displayed in cells. (B) Correlation structure for fold change data following OUMV models. (C) Linear relationship between mean expression within orthogroups and the OUMV parameter estimates for all reproductive modes and data types (expression and fold change).

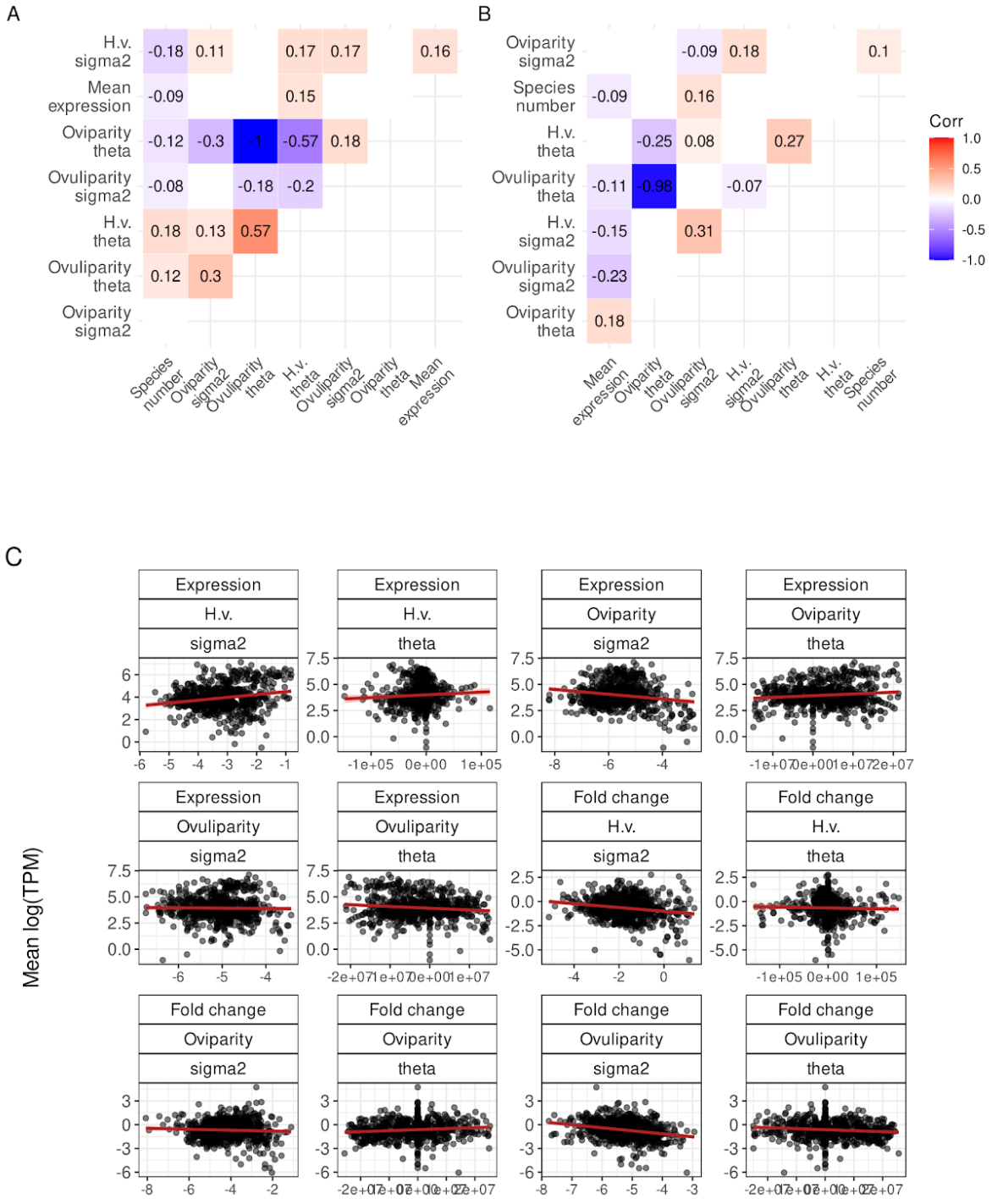

Suppl. Figure 20. Correlation structure of parameter estimates and other variables for BMS models. (A) Correlation structure for expression data following BMS models. Correlation coefficients without p-values < 0.05 are not displayed in cells. (B) Correlation structure for fold change data following BMS models. (C) Linear relationship between mean expression within orthogroups and the BMS parameter estimates for all reproductive modes and data types (expression and fold change).

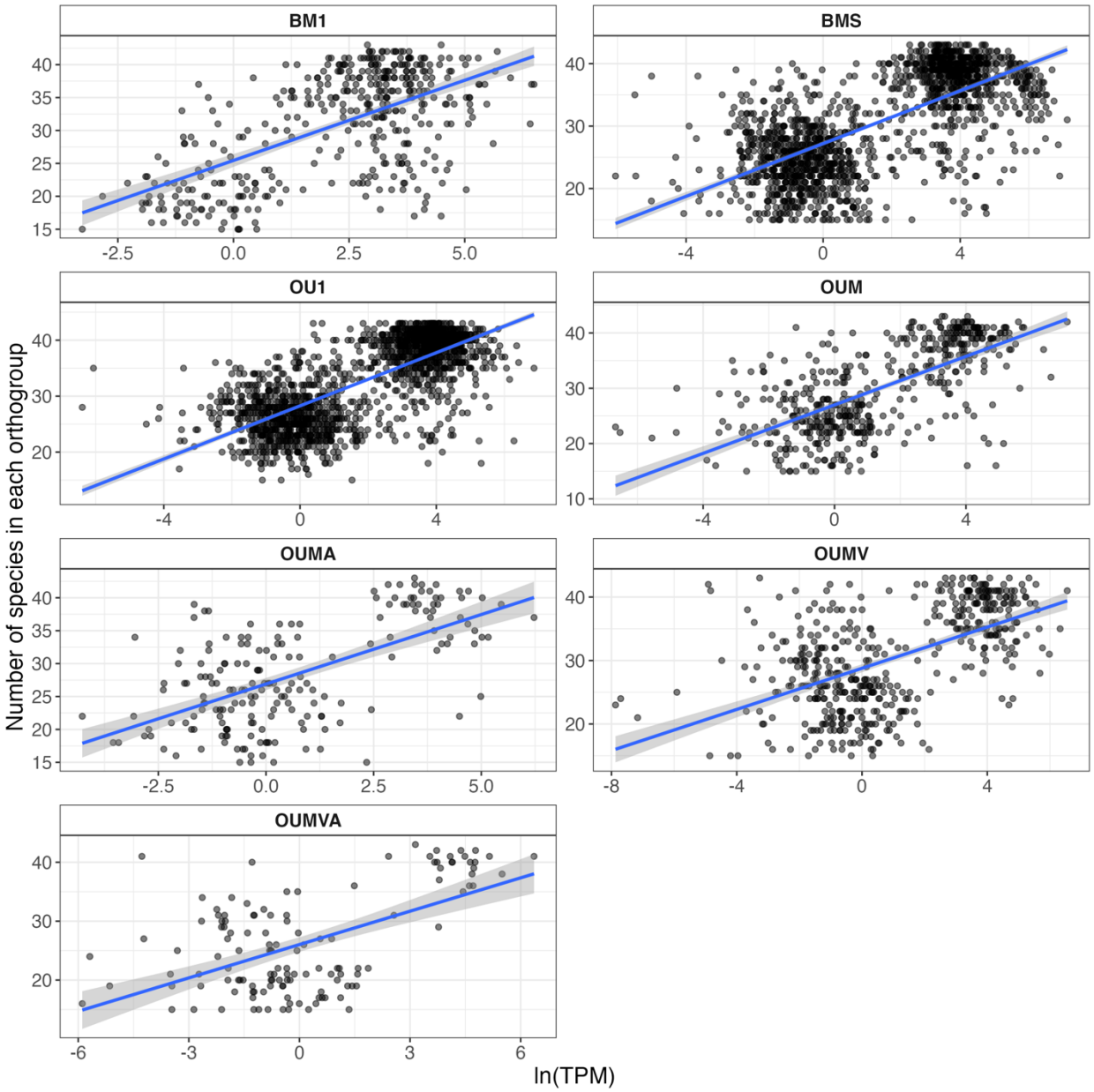

Suppl. Figure 21. Linear relationship depicted between mean expression values and number of species in each orthogroup. Each model is represented as a separate subplot. Standard linear model is represented by the blue line with confidence intervals represented as the gray area around the blue line.